A New Upper-Level Circulation Index for the East Asian Summer Monsoon Variability

GUIJIE ZHAO

State Key Laboratory of Numerical Modeling for Atmospheric Sciences and Geophysical Fluid Dynamics, Institute of Atmospheric Physics, Chinese Academy of Sciences, and College of Earth Science, University of Chinese Academy of Sciences, Beijing, China

GANG HUANG

State Key Laboratory of Numerical Modeling for Atmospheric Sciences and Geophysical Fluid Dynamics, Institute of Atmospheric Physics, Chinese Academy of Sciences, and Joint Center for Global Change Studies, Beijing, China

RENGUANG WU, WEICHEN TAO, HAINAN GONG, XIA QU, AND KAIMING HU

Center for Monsoon System Research, Institute of Atmospheric Physics, Chinese Academy of Sciences, Beijing, China

(Manuscript received 8 April 2015, in final form 16 September 2015)

ABSTRACT

The East Asian summer monsoon (EASM) and its variability involve circulation systems in both the tropics and midlatitudes as well as in both the lower and upper troposphere. Considering this fact, a new EASM index (NEWI) is proposed based on 200-hPa zonal wind, which takes into account wind anomalies in the southern (about 5°N), middle (about 20°N), and northern areas (about 35°N) of East Asia. The NEWI can capture the interannual EASM-related climate anomalies and the interdecadal variability well. Compared to previous indices, the NEWI shows a better performance in describing precipitation and air temperature variations over East Asia. It can also show distinct climate anomalous features in early and late summer. The NEWI is tightly associated with the East Asian–Pacific or the Pacific–Japan teleconnection, suggesting a possible role of internal dynamics in the EASM variability. Meanwhile, the NEWI is significantly linked to El Niño–Southern Oscillation and tropical Indian Ocean sea surface temperature anomalies. Furthermore, the NEWI is highly predictable in the ENSEMBLES models, indicating its advantage for operational prediction of the EASM. The physical mechanism of the EASM variability as represented by the NEWI is also explicit. Both warm advection anomalies of temperature by anomalous westerly winds and the advection of anomalous positive relative vorticity by northerly basic winds cause anomalous ascending motion over the mei-yu–changma–baiu rainfall area, and vice versa over the South China Sea area. Hence, this NEWI would be a good choice to study, monitor, and predict the EASM.

1. Introduction

The East Asian summer monsoon (EASM) is one of the most energetic components of Earth's climate system during boreal summer. Accumulated researches have indicated that the variability of the EASM has substantial social and economic influences (Rodwell and Hoskins 2001; Jiang et al. 2008). For example, an anomalous EASM can cause flood and high temperature extremes (Jiang et al. 2008; Hu et al. 2011, 2013). It is still a great challenge to predict the EASM and associated climate features accurately (B. Wang et al. 2001).

Indices are an important tool for the study of the EASM, and many EASM indices (EASMIs) have been proposed based on different variables at different levels with different purposes. Wang et al. (2008) have compared and classified these indices into five categories: the east–west thermal contrast index (Guo 1983; Shi and Zhu 1996; Peng et al. 2000; Zhao and Zhou 2009), the north–south thermal contrast index (Webster and Yang 1992; Zhu et al. 2000), the shear vorticity index (Huang and Yan 1999; Wang and Fan 1999; Lau et al. 2000; Zhang et al. 2003; Xie et al. 2009), the southwest monsoon index (Wu and Ni 1997; Y. Wang et al. 2001), and

Corresponding author address: Gang Huang, State Key Laboratory of Numerical Modeling for Atmospheric Sciences and Geophysical Fluid Dynamics, Institute of Atmospheric Physics, Chinese Academy of Sciences, Beijing 100029, China.
E-mail: hg@mail.iap.ac.cn.

DOI: 10.1175/JCLI-D-15-0272.1

the South China Sea monsoon index (Dai et al. 2000). These five groups of indices, to some extent, reflect the current understanding of the EASM variability. These indices mentioned in Wang et al. (2008) have been used to depict the characteristics of the EASM and associated climate. Yet, some problems exist. For instance, the rainfall and temperature anomalies represented by the Lee–Jhun–Park index (LJPI) (Lee et al. 2005) display an eastward shift as this is a northeast Asian summer monsoon index (see section 4; Fig. 5b). Sea level pressure (SLP)-based indices such as the Guo index (GQYI) (Guo 1983), Shi–Zhu index (SZI) (Shi and Zhu 1996), and Zhao–Zhou index (ZZI) (Zhao and Zhou 2009) could not represent the precipitation and temperature variations over East Asia properly (Figs. 5c–e), which is probably because the SLP is affected by some weather processes around the surface. The Wang–Fan index (WFI) (Wang and Fan 1999) largely reflects features in the tropics and has a relatively weak relationship with temperature variations in the East Asia, especially northern East Asia (Fig. 5k), likely because this index mainly considers the low latitudes with relatively weak emphasis on the midlatitudes. The Lau–Kim–Yang index (LKYI) (Lau et al. 2000) could not represent climate variability in East Asia after the 1980s. Therefore, a new EASM index needs to be put forward. Such an index should depict properly features in both tropical and middle latitude areas as well as at both lower and upper troposphere associated with the variability of the EASM. It should capture not only multiscale variations, but also physical processes of the EASM. Such an index should also be predictable for the benefit of monitoring and prediction of climate anomalies associated with the EASM variability. The simplicity for construction and its capacity for prediction should also be taken into account, and so direct observable variables are preferable. In view of these considerations, the upper-level wind field may be a good choice as it is relatively less affected by complex weather processes near the surface.

Prominent circulation systems exit at different levels in association with the EASM. In the upper troposphere, a double-jet structure exists over the Eurasian continent, which is in geostrophic balance with temperature gradients over the midlatitudes and along the coastline of the Arctic Sea (Hirota and Takahashi 2012). In the middle troposphere, a dominant system is the western Pacific subtropical high, which greatly influences climate anomalies in East Asia (Chen et al. 1992). In the lower troposphere, there is an anticyclone over the northwestern Pacific whose location change is closely related to summer rainfall anomalies in East Asia (He et al. 2007). The EASM has distinct features at different levels and complex spatial and temporal structures encompassing the tropics, subtropics, and midlatitudes (Murakami and Matsumoto 1994). Thus, a good index to measure the EASM variability needs to take into account properly not only related features over the midlatitudes, but also those over the tropics as well as at both lower and upper troposphere.

At 200 hPa, the East Asian jet stream (EAJ) is one important part of the EASM system (Tao and Wei 2006; Huang et al. 2012; Qu and Huang 2012). The westerly jet is located in midlatitudes with the wind speed reaching maximum at upper troposphere. The jet axis is approximately along 40°N, extending from northwestern China through northern China to the Korea Peninsula and north-central Japan. The EAJ has a great influence on weather and climate around East Asia. Its significant seasonal movement is closely linked to the outbreak of the East Asian monsoon and the movement of the rain belt of East Asian subtropical region (Tao and Chen 1957). The association of the East Asian upper-level jet with EASM has been mentioned in previous studies (e.g., Lau and Li 1984; Liang and Wang 1998; Kwon et al. 2007). The mei-yu period around the Yangtze River valley is greatly impacted by the EAJ (Du et al. 2008). Furthermore, precipitation can influence the intensity of EAJ in return (Kwon et al. 2007). The EAJ is intimately related to the EASM so we can use the upper-level wind to represent the EASM. Dai et al. (2013) found that summer thermal structure and winds over Asia show a larger land–ocean thermal gradient in the upper than in the lower troposphere. This implies a bigger role of the upper troposphere in driving the Asian summer monsoon circulation.

As we all know, the mei-yu–changma–baiu rainfall is one of the key components of EASM. To define the main rain belt in June–August (JJA) in East Asia, we perform an EOF analysis based on the JJA-mean precipitation anomalies over the domain of East Asia about 0°–60°N, 100°–160°E. Figures 1a and 1b show the first and second EOF modes of the summer-mean precipitation anomalies, respectively. Two distinct rain belts are detected: one is the mei-yu–changma–baiu rainband (27.5°–32.5°N, 105°–120°E and 30°–37.5°N, 127.5°–150°E) and the other the tropical Philippine Sea rainband (10°–20°N, 115°–150°E). On the interannual time scale, the variability of the two rainbands is large as revealed by the standard deviation of precipitation (Fig. 1c). The mei-yu–changma–baiu rain belt is one of the prominent features of the EASM. Alternatively, it has been called the East Asian monsoon trough since it is the main low-level convergence region over East Asia that produces most of the summer monsoon rainfall (Chen and Chang 1980). For the purpose of taking into consideration both lower and upper tropospheric

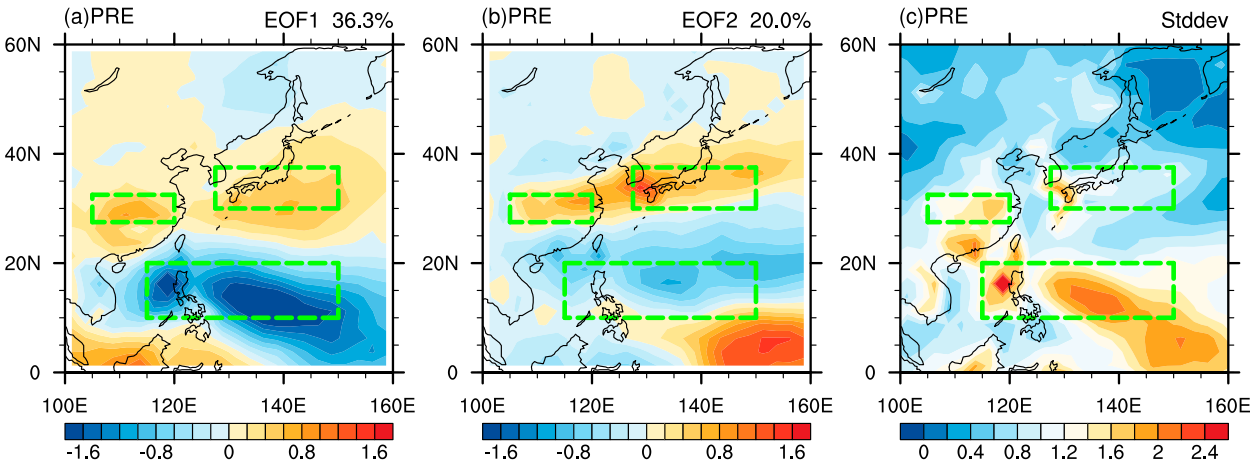

FIG. 1. The (a) first and (b) second EOF modes of JJA-mean precipitation anomalies (mm day^{-1}; color shading). (c) The distribution of the standard deviation of JJA-mean precipitation (mm day^{-1}; color shading). The time period is 1958–2013. The mei-yu–changma–baiu rainfall area refers to 27.5°–32.5°N, 105°–120°E and 30°–37.5°N, 127.5°–150°E; the tropical Philippine Sea rainfall area refers to 10°–20°N, 115°–150°E marked by the dashed green rectangles.

physical processes to depict the variability of EASM, we compute the JJA regression between the mei-yu–changma–baiu rainfall and zonal wind. From Fig. 2a, the 200-hPa zonal wind has the most significant correlation with the mei-yu–changma–baiu rainfall. The correlation with tropical Philippine Sea rainfall displays similar feature. Based on this, 200-hPa zonal wind is strongly linked to low-level processes and is capable of measuring the variability of EASM.

Lau et al. (2000) proposed an EASM index based on 200-hPa zonal wind, defined as LKYI = u(40°–50°N, 110°–150°E) − u(25°–35°N, 110°–150°E). Yet, this index does not include the wind over low latitudes, leading to its poor performance in depicting the East Asian climate after the 1980s (figure not shown). It has been shown that the convection activities around the Philippine Sea area have great influence on the activity of EASM (Yang and Webster 1990; Li et al. 2013) through the East Asian–Pacific (EAP; Huang and Wu 1989) or Pacific–Japan (PJ; Nitta 1987; Kosaka and Nakamura 2010) teleconnection. From this perspective of view, it is necessary to take into account of 200-hPa zonal wind in both the tropics and subtropics.

As the 200-hPa zonal wind is strongly linked to low-level processes and is capable of measuring the variability of EASM, in this study, we propose a new EASM index (NEWI) based on 200-hPa zonal wind. The wind anomalies not only in the northern and central areas but also in the south from the mean state above the East Asia area are taken into account. As we all know, the atmospheric processes in both the middle and high latitudes and the tropical ocean play an important role in the variability of the EASM. Thus, we take both the tropical and subtropical wind changes into account when defining the NEWI. The NEWI needs to reflect reasonably both the precipitation and temperature variability associated with the EASM. Following the suggestion by Wang et al. (2008), a strong EASM indicates an excessive rainfall in the mei-yu–changma–baiu area.

The rest of this paper is organized as follows. Section 2 describes the datasets and methods used in our study. Section 3 defines the NEWI. Section 4 then delineates the precipitation and temperature circulation anomalies represented by the NEWI. Section 5 gives the associations with sea surface temperature (SST) and potential predictability of the index. In this section, we also assess the predictability of the NEWI by examining the predictions in ENSEMBLES. We also compare the NEWI with some selected typical EASM indices in the past in sections 4 and 5. The physical mechanism of the NEWI is illustrated in section 6. Finally, a discussion and summary are provided in section 7.

2. Data and methods

The datasets used in this study include the following products: (i) the Japanese 55-year Reanalysis Project (JRA-55; Kobayashi et al. 2015) data, with a 1.25° × 1.25° horizontal resolution and from 1000 to 1 hPa with 37 vertical pressure levels; (ii) the Extended Reconstructed Sea Surface Temperature (ERSST; Smith et al. 2007), version 3.0 data, with a 2° × 2° horizontal resolution; and (iii) the monthly global Precipitation Reconstruction (PREC; Chen et al. 2002) dataset, with a 2.5° × 2.5° horizontal resolution. We also use the monthly-mean

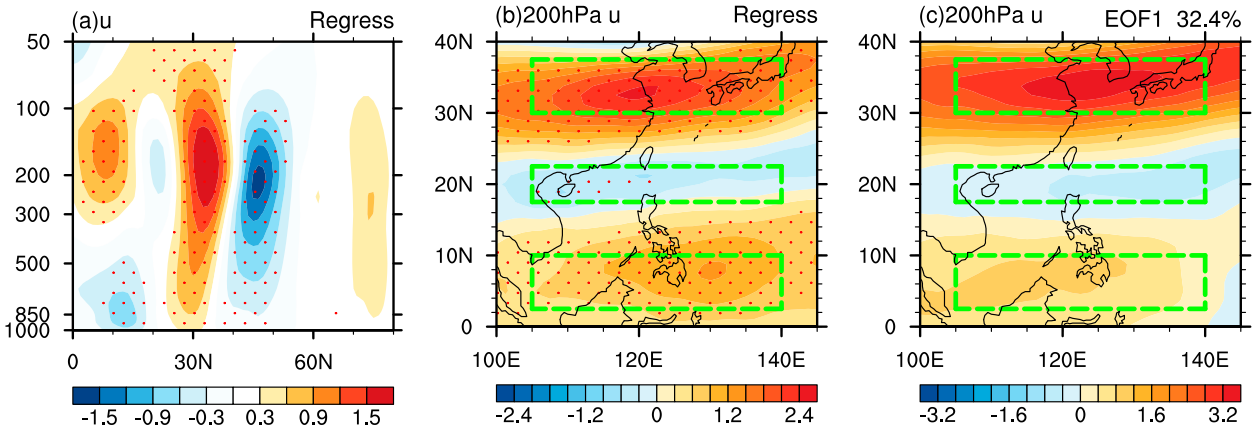

FIG. 2. (a) Latitude–height cross section showing regression anomalies (color shading) of zonal wind averaged between 105° and 150°E ($m\,s^{-1}$) against JJA-mean mei-yu–changma–baiu rainfall, (b) regression anomalies (color shading) of 200-hPa zonal wind ($m\,s^{-1}$) against JJA-mean mei-yu–changma–baiu, and (c) the first EOF mode of JJA-mean 200-hPa zonal wind anomalies ($m\,s^{-1}$; color shading). The red dots indicate the 95% confidence levels based on a two-sided Student's *t* test. The dashed green rectangles indicate the areas used to define the NEWI. The time period is 1958–2013.

surface air temperature and precipitation from 756 Chinese stations provided by the China Meteorological Administration. This dataset starts from 1951 and updates every month to the present. The focus period is 1958–2013.

To understand the contribution of the SST change to the observed variation of the EASM, two atmospheric general circulation models (AGCMs) are employed: the Hamburg version of the European Centre for Medium-Range Weather Forecasts model, version 5 (ECHAM5), and the Community Atmosphere Model, version 3 (CAM3) (Collins et al. 2006). The resolutions of the two AGCMs are spectral triangular truncation at wavenumber 63 and 19 vertical levels (T63L19) and spectral triangular truncation at wavenumber 42 and 26 vertical levels (T42L26), respectively. The AGCMs are driven by global historical Hadley Centre Sea Ice and SST (HadISST1) data. A 17-member ensemble simulation is conducted with ECHAM5 for 1871–2007 and a 21-member ensemble simulation with CAM3 for 1950–2000. The initial condition of each member is different. The ensemble means are used in the analysis to minimize the internal variability of the AGCMs and the error due to initial conditions. We use these model simulation data from 1958–2000 in this study.

ENSEMBLES [an European Union (EU)-funded integrated project] intends to develop an ensemble prediction system for climate change based on the five state-of-the-art coupled models developed in Europe for the period of 1960–2005 (Li et al. 2012). The models include the Met Office (UKMO), Météo-France (MF), the European Centre for Medium-Range Weather Forecasts (ECMWF), the Leibniz Institute of Marine Sciences at Kiel University (IFM-GEOMAR), and the Centro Euro-Mediterraneo per I Cambiamenti Climatici–Istituto Nazionale di Geofisica e Vulcanologia (CMCC-INGV). Further details of the ENSEMBLES multimodel project and the models are available in Doblas-Reyes et al. (2009). The retrospective forecasts (hindcasts) of all five models have been performed for a 46-yr period of 1960–2005. For each year, the seasonal forecasts are initialized on 1 May and run for seven months with nine members for each model. The multimodel ensemble (MME) results are calculated through simple composite by applying equal weights to all five models.

Here, the summer mean refers to the JJA mean. Analysis methods mainly include physical analysis, correlation analysis, regression analysis, and empirical orthogonal function (EOF) analysis. The significance levels are evaluated with the standard two-tailed Student's *t* test.

3. Definition of the new EASM index

According to the discussion in the introduction, we try to find out a new index depicting the EASM variability from the upper-troposphere wind. We first compute the JJA regression between the mei-yu–changma–baiu rainfall and 200-hPa zonal wind. Figure 2b reveals a distinct "positive–negative–positive" pattern with three significant bands. Three centers are located about 5°, 20°, and 35°N, respectively. The 200-hPa zonal wind pattern regressed against the tropical Philippine Sea rainfall leads to similar distribution (figure not shown). To confirm whether the above regions have large variation, we perform an EOF analysis based on the JJA-mean

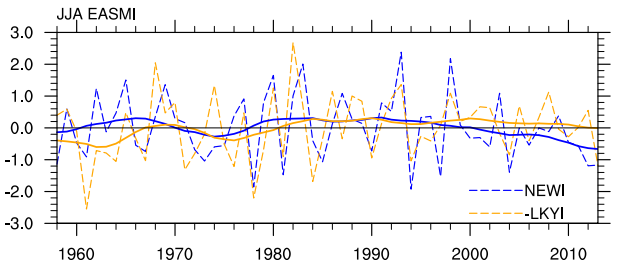

FIG. 3. Normalized JJA-mean EASMI (dashed lines) and 11-yr running average (solid lines) for the period 1958–2013. The blue lines are for the NEWI, and the orange lines are for the reversed LKYI.

200-hPa zonal wind anomalies over the domain of East Asia about 0°–40°N, 100°–145°E. Figure 2c shows the first EOF mode of the summer-mean 200-hPa zonal wind anomalies. The first mode explains 32.4% of the total variance in summer. It also reveals a distinct positive–negative–positive pattern, with the centers of these three bands located about 5°, 20°, and 35°N, respectively. Among these three centers, the center located around 35°N has the largest loading. We have also tried the EOF analysis for larger domains and the obtained results are similar. Comparing Figs. 2b and 2c, considering both the precipitation pattern in the low levels and the circulation mode in the upper levels, an EASM index is proposed as below:

$$\begin{aligned}\mathrm{NEWI} = \mathrm{Nor}[&u(2.5°–10°\mathrm{N}, 105°–140°\mathrm{E})\\ &- u(17.5°–22.5°\mathrm{N}, 105°–140°\mathrm{E})\\ &+ u(30°–37.5°\mathrm{N}, 105°–140°\mathrm{E})],\end{aligned}$$

where Nor represents standardization and u is JJA-mean 200-hPa zonal wind. When easterly anomalies appear around 20°N and westerly anomalies appear around 5° and 35°N, the index is positive, and the EASM is stronger.

There has been a lot of research on the interdecadal variability of EASM. Following the definition of a strong EASM index suggested by Wang et al. (2008), the EASM circulation has exhibited a strengthening tendency in the late 1970s (Hsu et al. 2014). Recent studies found that the EASM has been weakening since the early 1990s (Liu et al. 2012). Observational analyses reveal a weaker monsoon index from 1910 to 1970 and an enhancing monsoon since the late 1970s (Zhou et al. 2009). Figure 3 shows the normalized EASM index for the period 1958–2013. It features prominent interannual variations and captures the decadal strengthening of the EASM around the late 1970s. After 2000, the EASM begins to weaken. We also compare the NEWI with some widely used indices such as the LKYI and Huang–Yan index (HYI) (Huang and Yan 1999). These indices show similar interdecadal and interannual variability. Besides, the NEWI can detect that, when the decadal EASM is under the background of high index for the period from the late 1970s to the late 1990s, the amplitude of the index is likely to be large, indicating active interannual variability of the EASM.

4. Anomalies represented by the EASM index

a. Precipitation and temperature

Precipitation and temperature are the two most significant elements of the EASM. To analyze the capacity of the NEWI for representing the East Asian summer climate anomalies, we analyze the relationship of precipitation and temperature with the index. When the index is above average, precipitation anomalies display zonally elongated distribution, with suppressed rainfall over the South China Sea extending eastward and increased rainfall extending from the Yangtze River valley crossing the Korea Peninsula to Japan (Fig. 4a). The distribution of temperature anomalies shows a similar feature except that the temperature and precipitation anomalies are opposite, which is a typical feature over East Asia in summer (Wu et al. 2013). There are large areas of negative anomalies distributed in northern Asia. The precipitation and temperature patterns are similar to the leading modes of rainfall (Figs. 1a,b) and temperature anomalies (figures not shown) over East Asia. This reveals that the NEWI can capture the dominant modes of rainfall and temperature variations in summer over East Asia. The NEWI can also capture the seasonal shift of the mei-yu–changma–baiu rain belt (figure not shown).

To compare the NEWI with previous EASMIs, we first perform the regression analysis of different EASMIs with precipitation and temperature. We choose 15 previous EASMIs defined by different variables including the rainfall, the SLP, the geopotential height (hgt), and the wind. The descriptions of these indices are presented in Table 1. These selected indices are simple for construction, representative, and widely known. The SLP-based indices, such as the GQYI, SZI, and ZZI, show weak association with precipitation and temperature over East Asia (Figs. 5c–e). Some other indices including the PSNI, WYI, and WNI do not reflect precipitation and temperature anomalies so well (Figs. 5g,h,o). Although the rainfall-based index, the 850-hPa zonal wind–based indices, and the surface zonal wind–based index obtain a good relationship with precipitation, their capacity to represent the related temperature anomalies is limited (the LJPI, WFI, DXZI, ZTCI, and XHHI; Figs. 5b,k,l,m,j). The ZHWI and WWOI's descriptions

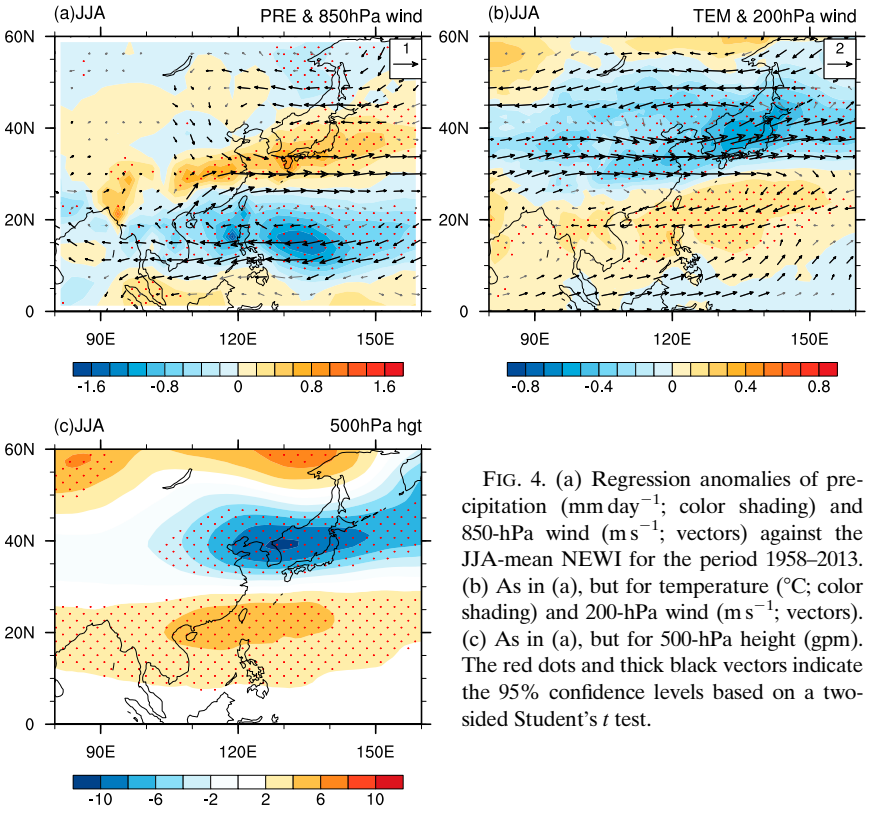

FIG. 4. (a) Regression anomalies of precipitation (mm day^{-1}; color shading) and 850-hPa wind (m s^{-1}; vectors) against the JJA-mean NEWI for the period 1958–2013. (b) As in (a), but for temperature (°C; color shading) and 200-hPa wind (m s^{-1}; vectors). (c) As in (a), but for 500-hPa height (gpm). The red dots and thick black vectors indicate the 95% confidence levels based on a two-sided Student's *t* test.

of precipitation and temperature anomalies are relatively good, but not as good as the NEWI (Figs. 5i,p). The HYI's depiction of precipitation anomalies is slightly worse than the NEWI, and its depiction of temperature anomalies is not so good in northwestern China (Fig. 5f). Finally, the LKYI depicts precipitation anomalies slightly worse than the NEWI, and its representation of temperature anomalies in northwestern China is not so good (Fig. 5n).

The amount of precipitation is the most direct measure of monsoon activity. The mei-yu–changma–baiu system is the most important rainfall-producing agent of the EASM and therefore the most important provider of the heat source that drives the EASM (Wang et al. 2008). So we use the indices' correlations with precipitation in the mei-yu–changma–baiu rainfall area to further examine the indices' performance in capturing the EASM characteristics. We compute the correlation coefficient between the EASMI and the mei-yu–changma–baiu rainfall, which is shown in Table 1. Among all these 16 indices, the NEWI has the second-best relationship with precipitation in the mei-yu–changma–baiu rainfall area, second only to the LJPI. However, the LJPI mainly obtains the features over northeastern Asia and also its capability of representing temperature variation is limited (Fig. 5b). Meanwhile, the three SLP-based indices, PSNI, and WYI have poor relationship, and the other indices are well correlated with the precipitation although less well than the NEWI. These results are consistent with the above regression analysis.

Furthermore, we verify the above results utilizing the 756 stations data in China. We calculated the correlation coefficients between the indices listed in Table 1 and the 756 stations' JJA-mean precipitation and temperature in China for the period 1958–2013. The numbers of stations with the correlation coefficient exceeding the 99%, 95%, and 90% confidence levels are compared (data not shown). The results are in accordance with the regression and correlation results above. The NEWI has the most stations exceeding the different levels of confidence. Therefore, the NEWI can better capture precipitation and temperature characteristics over East Asia.

b. Circulation system

The distribution of precipitation and temperature anomalies is influenced by atmospheric circulation and the atmospheric circulation is an important factor of the EASM system. Thus, we analyze the vertical structure of circulation anomalies associated with the NEWI. The dominant feature in the cross section

TABLE 1. Description of the NEWI and 15 EASM circulation indices. For defining variables, pre is precipitation, u is zonal wind, v is meridional wind, and hgt is geopotential height. Their correlation coefficients with the precipitation in the mei-yu–changma–baiu rainfall area (27.5°–32.5°N, 105°–120°E and 30°–37.5°N, 127.5°–150°E) for the period 1958–2013 are shown. One and two asterisks indicate that the correlation coefficients exceed the 99% and 99.9% confidence levels based on a two-sided Student's t test, respectively.

Index	Reference	Defining variable; level (hPa); and region	Correlation coef
NEWI		u; 200; 2.5°–37.5°N, 105°–140°E	0.65**
LJPI	Lee et al. (2005)	pre; surface; 20°–50°N, 100°E –180°	0.87**
GQYI	Guo (1983)	SLP; surface; 10°–50°N, 110°–160°E	−0.14
SZI	Shi and Zhu (1996)	SLP; surface; 20°–50°N, 110°–160°E	−0.19
ZZI	Zhao and Zhou (2009)	SLP; surface; 30°–50°N, 110°–160°E	0.01
HYI	Huang and Yan (1999)	hgt; 500; 20°–60°N, 125°E	−0.54**
PSNI	Peng et al. (2000)	hgt; 500; 10°–50°N, 110°–150°E	0.10
WYI	Webster and Yang (1992)	u; 850–200; 0°–20°N, 40°–110°E	−0.10
ZHWI	Zhu et al. (2000)	u; 850–200; 0°–10°N, 100°–130°E SLP; surface; 10°–50°N, 110°–160°E	−0.32
XHHI	Xie et al. (2009)	u; surface; 10°–32.5°N, 120°–150°E	0.49**
WFI	Wang and Fan (1999)	u; 850; 5°–32.5°N, 90°–140°E	−0.49**
DXZI	Dai et al. (2000)	u; 850; 5°–15°N, 105°–120°E	−0.33
ZTCI	Zhang et al. (2003)	u; 850; 10°–35°N, 100°–150°E	−0.51**
LKYI	Lau et al. (2000)	u; 200; 25°–50°N, 110°–150°E	−0.55**
WNI	Wu and Ni (1997)	v; 850; 20°–30°N, 110°–130°E	0.29
WWOI	Y. Wang et al. (2001)	v, 850; 20°–40°N, 110°–140°E	0.49**

of zonal wind anomalies is a barotropic structure signaling a northward shift of the upper-tropospheric jet stream (Fig. 6a), which creates a strong local anomalous vorticity gradient. The zonal wind anomalies display alternative westerly and easterly anomalies in the meridional direction. The maximum wind speed anomalous centers are around 200 hPa with another wind speed anomalous center about 850 hPa at the latitude of 15°N.

The shift in the zonal wind anomalies is associated with strong equatorward flow anomalies between surface and 300 hPa and poleward flow anomalies above 300 hPa, just south of the zonal wind anomaly maximum (Fig. 6b). The meridional wind anomaly section presents a barotropic structure above 200 hPa and a baroclinic structure below 200 hPa (Fig. 6b).

The local latent heat–induced meridional circulation appears to be squeezed into a narrow latitudinal band with three centers at about 5°, 15°, and 30°N, respectively (Fig. 6c). The anomalous centers in the vertical velocity agree with the precipitation anomalies shown in Fig. 4a. The dominant feature in the cross section of geopotential height anomalies is also a barotropic structure signaling a northward shift of the upper-tropospheric jet stream (Fig. 6d).

For the purpose of understanding characteristics at different levels, we carry out regression analysis for different levels. Figure 4 shows atmospheric circulation anomalies at different levels. From the 850-hPa wind field (Fig. 4a), when there is a strong EASM, there are anomalous southwesterly flows carrying water vapor from the South China Sea to the mei-yu–changma–baiu rainfall area and anomalous northwesterly flows bringing relatively cold air from the midlatitudes there, leading to anomalous rain belt there. In addition, an anomalous anticyclone is situated over the northwestern Pacific with its center around 20°N, 130°E. The 200-hPa wind anomalies display obvious zonal distribution with westerly and easterly anomalies appearing alternately and the centers of anomalies are located about 5°, 20°, 35°, and 50°N (Fig. 4b). When a strong EASM occurs, easterly anomalies appear to the north and westerly anomalies to the south of the jet axis (near 40°N), resulting in the southward shift of the westerly jet. When there is a strong EASM, anomalous cyclone located around 40°N at 200 hPa, corresponding to the negative temperature anomalies in northern Asia (Fig. 4b).

From the 500-hPa geopotential height anomalies (Fig. 4c), northern China, Korea Peninsula, and Japan areas are located in the anomalous low pressure areas, and there are positive height anomalies in the northwestern Pacific subtropical high area when there is a strong EASM, corresponding to anomalous anticyclone at 850 hPa. The 500-hPa geopotential height anomalies present an EAP or PJ teleconnection pattern. The western Pacific subtropical high is a dominant feature in the middle troposphere and greatly influences the climate anomalies in East Asia.

From the above analyses, the NEWI can capture well the large-scale circulation features of the EASM at the lower, middle, and upper troposphere as

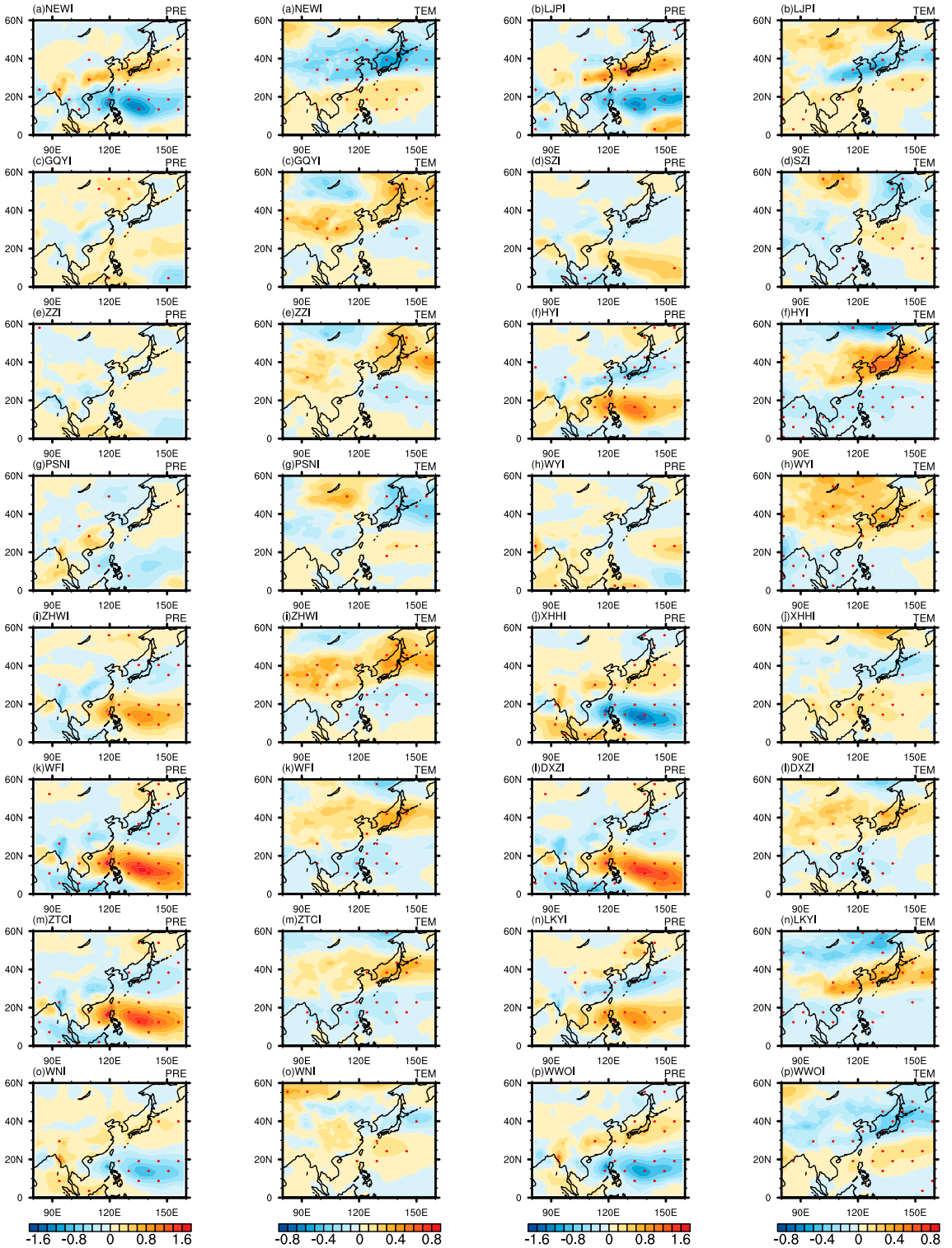

FIG. 5. (a) Regression anomalies (color shading) of (left) precipitation (mm day^{-1}) and (right) temperature (°C) against the JJA-mean NEWI for the period 1958–2013. (b)–(p) As in (a), but for the other 15 EASMIs. The red dots indicate the 95% confidence levels based on a two-sided Student's *t* test.

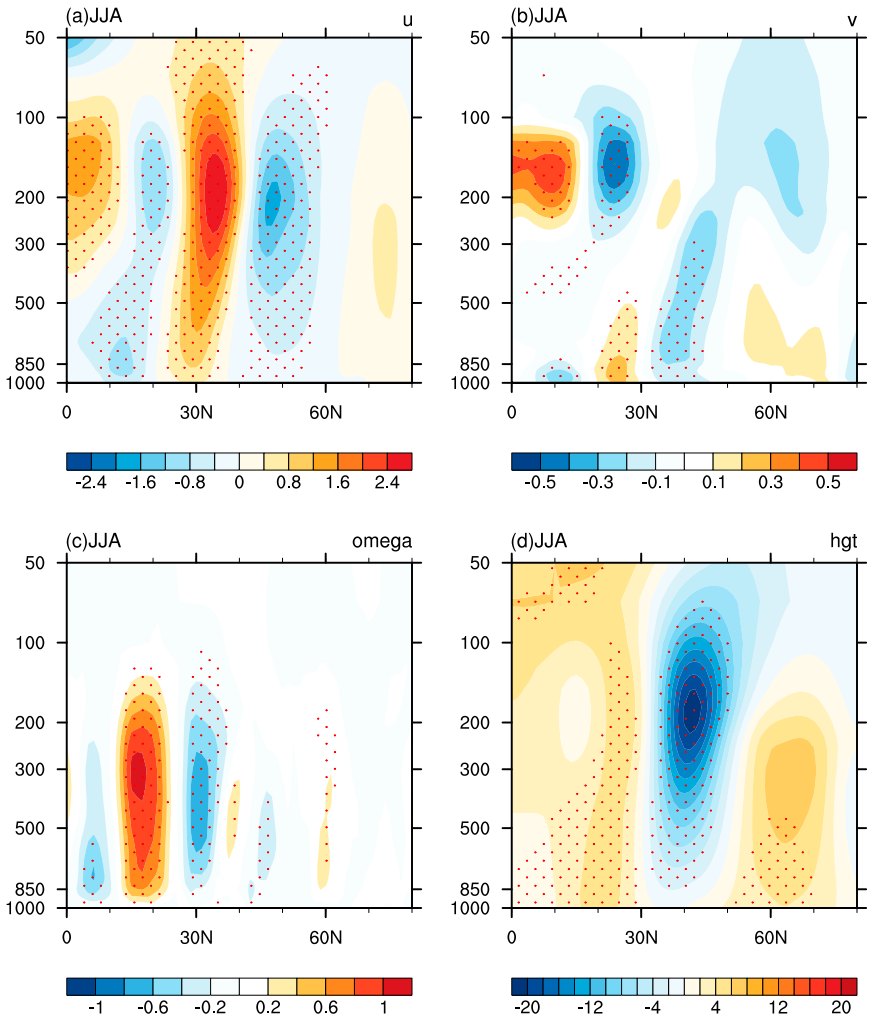

FIG. 6. Latitude–height cross section showing regression anomalies (color shading) of (a) zonal and (b) meridional wind ($m\,s^{-1}$), (c) vertical velocity ($hPa\,s^{-1}$), and (d) hgt (gpm) averaged between 105°–140°E against the JJA-mean NEWI for the period 1958–2013. The red dots indicate the 95% confidence levels based on a two-sided Student's *t* test.

revealed by previous studies (Ha et al. 2005; Wang et al. 2008). These circulation anomalies are closely associated with precipitation and temperature anomalies in the East Asia area corresponding to anomalous EASM.

c. *Anomalies in the early and late summer*

The rainy season over East Asia experiences the most spectacular northward march on earth during the period from May to August. Chang et al. (2000) divide the summer season into early summer and late summer. Also, as in Wang et al. (2009), the EASM can be divided into two subseasons: early summer [May and June (MJ)] and late summer [July and August (JA)]. There are pronounced differences in the subseasonal mean states between MJ and JA, and this is useful for the seasonal prediction of rainfall in East Asia. In this subsection, we divide the NEWI into MJ and JA to discuss the associated anomalies.

In MJ, precipitation anomalies are restricted in southern China and the area to south of Japan (Fig. 7a), whereas in JA the mei-yu–changma–baiu rain belt is obvious (Fig. 7b). The distribution of temperature anomalies shows a similar feature except that the temperature and precipitation anomalies are opposite. There are large areas of negative anomalies distributed in northwestern Asia in MJ and these move eastward in JA (Figs. 7c,d).

From Figs. 7a and 7b, the 850-hPa wind field is closely linked to the precipitation field. In MJ, the 850-hPa wind anomalies are mainly in the southern region, with an anomalous anticyclone situated over the northwestern Pacific with its center around 20°N, 130°E, while in JA,

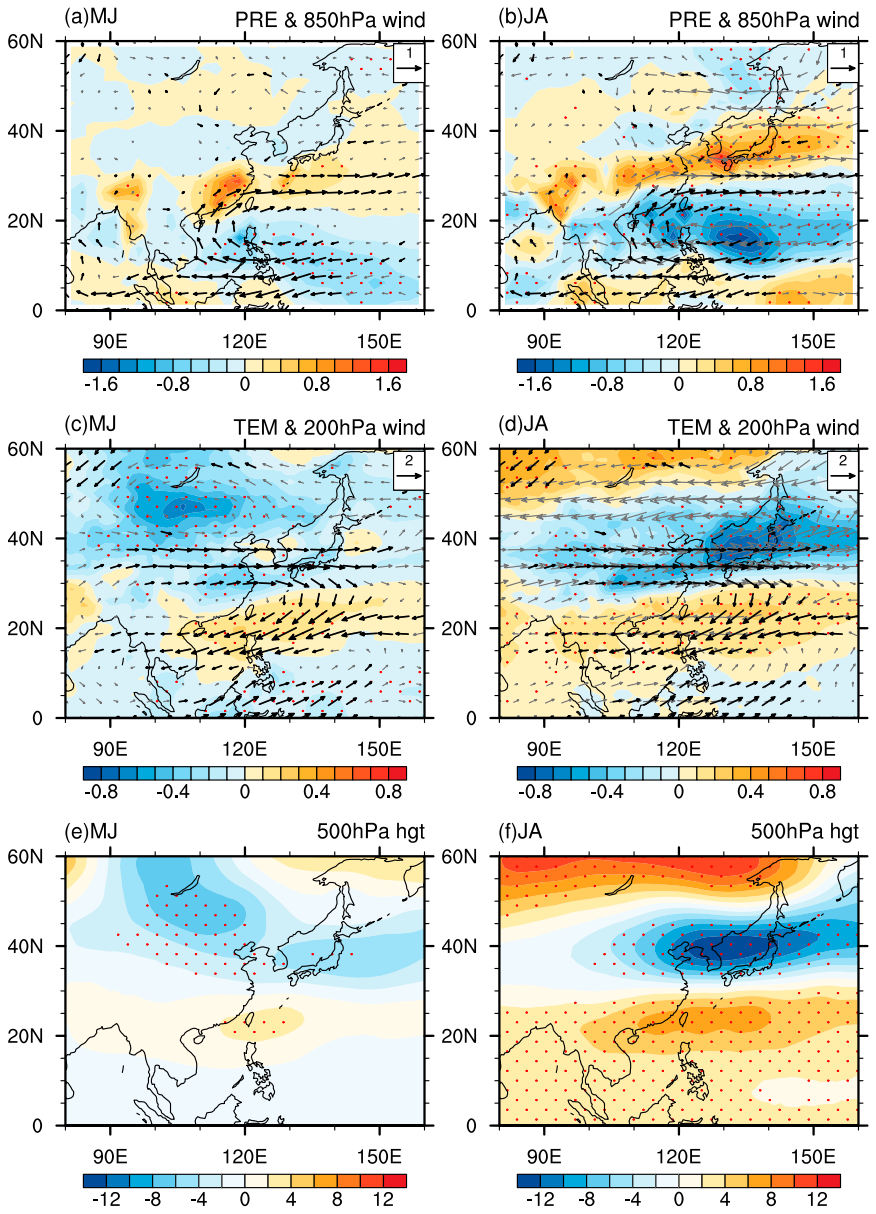

FIG. 7. As in Fig. 4, but regressed against the (a),(c),(e) MJ- and (b),(d),(f) JA-mean NEWI.

not only the anomalous anticyclone exists, but also an anomalous cyclone is situated in the northern region about 40°N, 130°E. The 200-hPa wind anomalies are associated with the temperature anomalies. In MJ, the anomalous centers are distributed from northwest to southeast (Fig. 7c), whereas in JA the anomalous centers are in the north–south direction with zonal elongation (Fig. 7d). From the 500-hPa geopotential height anomalies in MJ (Fig. 7e), there is no obvious EAP–PJ teleconnection pattern, whereas an EAP or PJ teleconnection pattern appears in JA (Fig. 7f). The NEWI can show the distinct climate anomalous features of early and late summer in East Asia.

5. Predictability of the EASM revealed by the new index

a. Observations

According to previous studies, the ocean is an important origin of the predictability of the EASM. The relationship between tropical SST and the East Asian monsoon has been the subject of many studies in the past decades (Chang et al. 2000). Shen and Lau (1995), using 1956–85 data, found a strong biennial signal in the correlations between EASM and the tropical SST. Moreover, the Niño-3.4 SST anomaly is an effective precursor for the western North Pacific (WNP)-EASM with a two-season

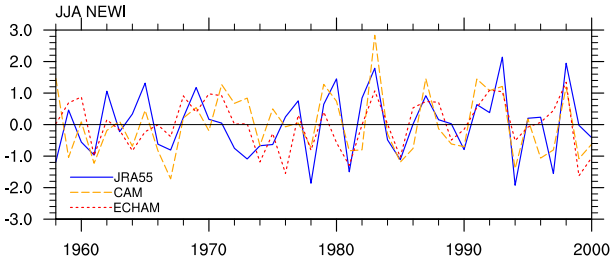

FIG. 8. Normalized JJA-mean NEWI from JRA-55 (blue solid line), CAM3 (orange dashed line), and ECHAM5 (red dotted line) for the period 1958–2000. The indices are detrended.

leading. Therefore, we analyze the relationship between the NEWI and SST in the following.

To investigate the contribution of ocean, we calculated the index from two AGCMs: CAM3 and ECHAM5 (Fig. 8). The correlation coefficient of the NEWI between the observation and CAM3 is 0.55, and that between the observation and ECHAM5 is 0.48 for the period 1958–2000, far more than the 99% significance level (0.39 for 41 degrees of freedom). The correlation between the observation and AGCMs has a big increase in the late 1970s corresponding to the decadal strengthening of the EASM.

We further carry out regression analysis of the NEWI with SST shown in Fig. 9. In the previous winter, the SST anomalous pattern displays an El Niño–like distribution with positive anomalies in the eastern Pacific and negative anomalies in the western Pacific (Fig. 9a). In the previous spring, the distribution is similar to the previous winter but the anomalies are somewhat smaller (Fig. 9b). Then in the summer, the positive anomalies in the eastern Pacific decrease to a small extent, and the northwestern Pacific reveals wavelike negative–positive–negative anomalies with the strongest anomalies in the north band (Fig. 9c). The north Indian Ocean displays positive anomalies. When the SST in the northwestern Pacific is colder in JJA, there is anomalous cyclone around 40°N, 130°E (Fig. 4a), and then a stronger EASM appears. When the eastern Pacific SST is warmer in the previous winter and the north Indian SST is warmer in the summer, a strong EASM probably appears. Also, in the previous winter, the central and eastern tropical Pacific SST anomalies are large, and they become smaller in the previous spring. In summer, the North Pacific SST anomalies are larger than in other seasons (figure not shown). These results are consistent with previous studies (Shen and Lau 1995; Chang et al. 2000; Wang et al. 2000). The Pacific SST can affect the Indian Ocean and then have influence on the East Asian climate through the Indian Ocean capacitor effect (Xie et al. 2009). The Pacific SST and the Indian Ocean SST

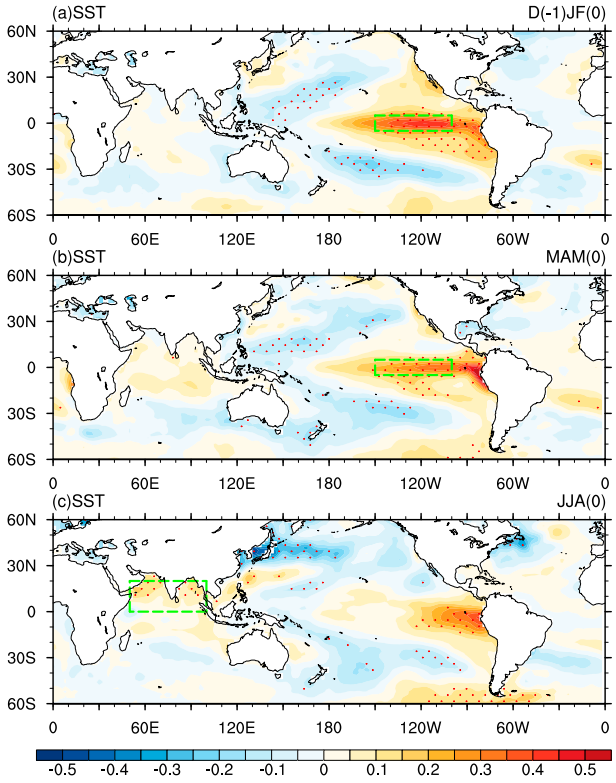

FIG. 9. (a) Regression anomalies (color shading) of December–February mean SST (°C) against the JJA-mean NEWI for the period 1958–2013. (b),(c) As in (a), but for March–May and June–August mean SST, respectively. The red dots indicate the 95% confidence levels based on a two-sided Student's *t* test. The tropical eastern Pacific area refers to 5°S–5°N, 150°–100°W; the north Indian Ocean area refers to 0°–20°N, 50°–100°E marked by dashed green rectangles.

anomalies both have impacts on the northwestern Pacific anticyclone, which has a great influence on East Asian climate (Wang et al. 2000; Yun et al. 2008; Lin and Lu 2009; Xie et al. 2009; Chu et al. 2012; Oh and Ha 2015).

From the above analysis, we choose two areas that are highly correlated with the NEWI: one in the tropical eastern Pacific (TEP; 5°S–5°N, 100°–150°W) and one in the north Indian Ocean (NIO; 0°–20°N, 50°–100°E) to analyze the SST's relationship with the NEWI in detail. The tropical eastern Pacific SST has a 4-month lead when the correlation coefficient reaches the maximum and the north Indian Ocean has a 1-month lead (Fig. 10). The Pacific SST's relationship with NEWI is better than the Indian Ocean's. Hence we can use the previous February–April TEP SST and May–July NIO SST to predict the EASM.

b. Simulations

We would like to know the models' simulating ability for this NEWI. Li et al. (2012) have used the ENSEMBLES data to study the predictability of the

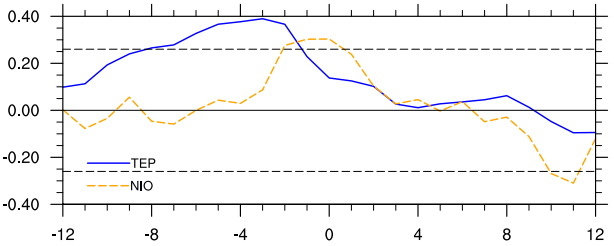

FIG. 10. Lead–lag correlations between the NEWI and SST anomalies averaged over the TEP (blue solid line) and the NIO (orange dashed line). The 95% confidence level for 54 degrees of freedom is 0.26.

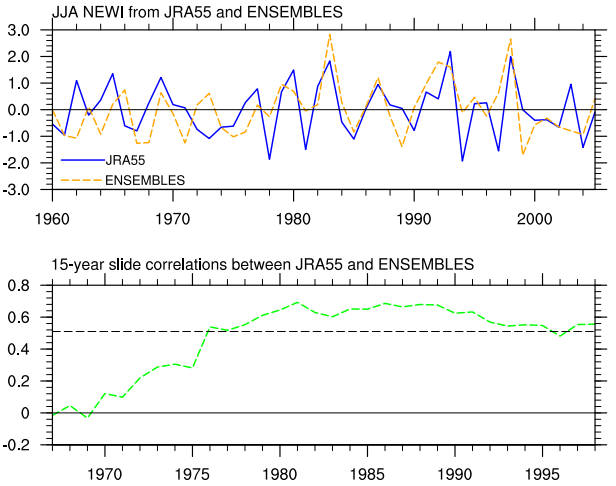

FIG. 11. (top) Normalized JJA-mean NEWI from JRA-55 (blue solid line) and ENSEMBLES (orange dashed line) for the period 1960–2005. (bottom) The 15-yr sliding correlation between NEWI from JRA-55 and ENSEMBLES. The 95% confidence level for 13 degrees of freedom is 0.51 shown in the bottom panel.

WNP summer climate and found that the models in general successfully predict the interannual variation of the WNP summer climate. We choose the data predicted from May from the ENSEMBLES and calculate the NEWI, which is shown in the top panel of Fig. 11. The correlation coefficient between the observational and simulation is 0.46 for 46 years, far beyond the significance level of 99% (0.38 for 44 degrees of freedom). The forecast capacity for EASM in the models is relatively poor at the end of the 1960s and beginning of the 1970s, becomes better in the mid-1970s, and has been maintained at a higher level since then (Fig. 11, bottom). Thereby, the models predict well the EASM variations as measured by the NEWI.

Furthermore, we compared the models' performance ability of these indices mentioned above. From Table 2, we can see that the models' simulation ability of the NEWI is among the best ones, only slightly worse than WFI and HYI, which is probably because the WFI mainly represents the information from tropical regions and could be better simulated. The HYI uses just three points of information and also can be better predicted. Among the five models, the IFM-GEOMAR has the best simulation ability of the EASM.

6. Physical mechanism

This section examines the physical mechanism of the EASM variability as represented by the NEWI. The association between the EASM and the upper-troposphere jet stream has been widely studied (e.g., Lau and Li 1984; Liang and Wang 1998). The EAJ is closely connected to the heating of the Tibetan Plateau area and latent heat release of mei-yu–changma–baiu rains (Zhang and Kuang 2006; Zhang et al. 2006). Li et al. (2004) have found that the northward marches of the EAJ are connected to the reversal of upper-troposphere meridional temperature gradient in the south Asian continent. The Tibetan Plateau anchors monsoon convection and hence a midtropospheric temperature maximum (Li and Yanai 1996). Regarding this, the heating of the Tibetan Plateau plays an important role. Sampe and Xie (2010) chose 500-hPa horizontal winds, which are little affected by mei-yu–changma–baiu heating, revealing the westerly jet as an important factor for the mei-yu–changma–baiu. The present study suggests that the remote forcing represented by the midtropospheric warm advection determines the location and timing of the mei-yu–changma–baiu formation. Along the rainband, mean ascending motion corresponds well with a band of warm horizontal temperature advection in the midtroposphere throughout summer. This adiabatic induction of upward motion originates from the advection of warm air by the westerlies from the eastern flank of the Tibetan Plateau.

a. Diagnosis by the omega equation

Vertical motion is closely related with rainfall. Comparing the anomalous rainfall pattern shown in Fig. 4a with the anomalous vertical velocity associated with the NEWI shown in Fig. 6c, the descending and ascending motions correspond well to the suppressed rainfall over the South China Sea area and increased rainfall in the mei-yu–changma–baiu rainfall area, respectively. Here we can see that the vertical motions anomalies and the rainfall anomalies have a good corresponding relationship.

As we all know, the quasigeostrophic omega equation can be used to diagnose vertical motions. Kosaka and Nakamura (2010) have utilized the omega equation to analyze the Pacific–Japan pattern. In the following, we first use the quasigeostrophic omega equation [Eq. (1)] to diagnose the formation mechanism of the vertical motions. The equation is written as follows:

TABLE 2. Correlation coefficients between the observed and the five nine-run model simulations as well as the MME EASMI predicted from May for the period 1960–2005. We choose the six indices as they are well correlated with precipitation and temperature over East Asia and are also representative. One and two asterisks indicate that the correlation coefficients exceed the 99% and 99.9% confidence levels based on a two-sided Student's *t* test, respectively.

Index	MME	ECMWF	IFM-GEOMAR	MF	UKMO	CMCC-B
NEWI	0.46*	0.37	0.53**	0.29	0.36	0.32
HYI	0.53**	0.43*	0.61**	0.30	0.38*	0.42*
ZHWI	0.36	0.46*	0.42*	0.05	0.28	0.34
WFI	0.59**	0.53**	0.60**	0.50**	0.49**	0.47**
LKYI	0.29	0.12	0.18	0.04	0.33	0.21
WWOI	0.37	0.02	0.49**	0.26	0.31	0.33

$$\underbrace{\left(\sigma\nabla^2 + f^2\frac{\partial^2}{\partial p^2}\right)}_{\text{A}}\omega = \underbrace{f\frac{\partial}{\partial p}[\mathbf{V}_g\cdot\nabla(\zeta_g + f)]}_{\text{B}} + \underbrace{\frac{R}{p}\nabla^2(\mathbf{V}_g\cdot\nabla T)}_{\text{C}} - \underbrace{\frac{R}{c_p p}\nabla^2\frac{dQ}{dt}}_{\text{D}}, \tag{1}$$

where all operators and variables are of conventional usage in meteorology. The term on the left-hand side of Eq. (1) is the Laplacian of omega (term A) and approximately equivalent to omega multiplied by a negative coefficient. The terms on the right-hand side are the vertical differential of geostrophic absolute vorticity advection (term B), the Laplacian of geostrophic temperature advection (term C), and the Laplacian of diabatic heating (term D), respectively. Precipitation can release condensational heating, which will reinforce upward movement and then produce more precipitation in return. So in the following, we diagnose terms B and C.

We first investigate term B and find that when the vorticity advection increases with height, then upward motions will be generated. The change of the vorticity advection with height is the result of the joined action of the relative vorticity and planetary vorticity. From the horizontal advection anomalies of geostrophic absolute vorticity and upward vertical pressure velocity anomalies field (Fig. 12a), when a strong EASM occurs, there are negative vorticity advection anomalies over about 15°–25°N and positive vorticity advection anomalies over 25°–35°N in the upper level. The positive vorticity in the upper level leads to the increase of cyclonic vorticity, which destroys the balance of the wind and pressure field; then horizontal divergence is certain to arise due to the Coriolis force, and there will be a compensation upward movement to keep the conservation of mass. Similarly, downward motions appear when the vorticity advection decreases with height. The relative vorticity plays a decisive role while the planetary vorticity is an order of magnitude smaller than the relative vorticity, and the planetary vorticity plays an opposite role (Figs. 12c,d).

The geostrophic advection of temperature anomalies and upward velocity anomalies associated with the NEWI in JJA is shown in Fig. 12b. The region of upward motion anomalies closely follows the region of warm temperature advection anomalies. If a strong EASM occurs, there are warm advection anomalies of temperature around 35°N, resulting in the sufficient mei-yu–changma–baiu rainfall. On the other hand, there are cold advection anomalies of temperature around 20°N, and then deficient rainfall anomalies occur over the South China Sea and the northwestern Pacific.

Therefore, the above results show that both the vorticity and temperature advection anomalies in the upper level induce vertical movement anomalies, and then cause the rainfall and temperature anomalies over East Asia.

b. *Further decomposition of the omega equation*

With the purpose of making it clear which parts matter in the vorticity and temperature advection anomalies, Eq. (1) is further decomposed into a climate mean basic and its departure (Peixóto and Oort 1984). The perturbation omega equation can be expressed as

$$\left(\sigma\nabla^2 + f^2\frac{\partial^2}{\partial p^2}\right)\omega' = \underbrace{\left(f\frac{\partial}{\partial p}u_g'\frac{\partial\overline{\zeta_g}}{\partial x}\right)}_{\text{B1}} + \underbrace{\overline{u_g}\frac{\partial\zeta_g'}{\partial x}}_{\text{B2}} + \underbrace{u_g'\frac{\partial\zeta_g'}{\partial x}}_{\text{B3}} + \underbrace{v_g'\frac{\partial\overline{\zeta_g}}{\partial y}}_{\text{B4}} + \underbrace{\overline{v_g}\frac{\partial\zeta_g'}{\partial y}}_{\text{B5}} + \underbrace{v_g'\frac{\partial\zeta_g'}{\partial y}}_{\text{B6}} + \underbrace{v_g'\frac{\partial f}{\partial y}}_{\text{B7}}$$
$$+ \underbrace{\frac{R}{p}\nabla^2\left(u_g'\frac{\partial\overline{T}}{\partial x}\right)}_{\text{C1}} + \underbrace{\overline{u_g}\frac{\partial T'}{\partial x}}_{\text{C2}} + \underbrace{u_g'\frac{\partial T'}{\partial x}}_{\text{C3}} + \underbrace{v_g'\frac{\partial\overline{T}}{\partial y}}_{\text{C4}} + \underbrace{\overline{v_g}\frac{\partial T'}{\partial y}}_{\text{C5}} + \underbrace{v_g'\frac{\partial T'}{\partial y}}_{\text{C6}}, \tag{2}$$

where the variables with the overbar and prime represent the basic state and perturbation, respectively.

In the following, we choose 200 hPa to diagnose vertical motion anomalies by calculating the anomalies of each term on the right-hand side of Eq. (2) as denoted by terms B1–B7 and C1–C6 associated with the NEWI in domains 30°–37.5°N, 105°–140°E and 15°–22.5°N, 105°–140°E, respectively. Our purpose is to find out the main contributors to the vertical motion anomalies over the mei-yu–changma–baiu rainfall area and the South China Sea area.

As shown in Table 3, the results reveal that the terms B5 and C1 in Eq. (2) are two main contributors to the updraft anomalies over the mei-yu–changma–baiu rainfall area and to the downdraft anomalies over the South China Sea area. The term B5 is closely related to the advection of anomalous relative vorticity by the basic meridional flow. The term C1 is the advection of the basic-state temperature by anomalous zonal flow. The temperature advection plays a more important role. In addition, the advection anomalies are stronger in the north than in the south. Since the four advection terms are related to the basic-state wind, basic-state temperature and anomalous wind, and anomalous relative vorticity, their fields at 200 hPa are shown further illustrating of the effect of them on the vertical motions.

As shown in Fig. 13a, term B5 can be well reflected by the pattern of anomalous relative vorticity field, and there is obvious meridional gradient of anomalous relative vorticity. When the EASM is stronger, there are negative relative vorticity anomalies around 25°–30°N and positive anomalies around 40°N, resulting in negative vorticity advection anomalies around 20°N and positive vorticity advection anomalies around 35°N by the basic northerly wind component. In consequence, descending motion is located about 20°N and ascending motion about 35°N. In addition, the vorticity centers and the wind field shift northward from June to August, accompanying the shift of the rain belt (figures not shown).

On the other hand, term C1 can be well reflected by the pattern of anomalous circulation and basic temperature shown in Fig. 13b. There are westerly anomalies in the northern area and easterly anomalies in the southern area, along with negative zonal gradient of the basic temperature, resulting in the temperature advection anomalies. As shown in Figs. 12b and 13b, associated with the NEWI, if a strong EASM occurs there are westerly wind anomalies around 35°N, leading to anomalous warm temperature advection, resulting in sufficient mei-yu–changma–baiu rainfall. On the other hand, there are easterly wind anomalies around 20°N, leading to cold advection anomalies to the south of China. Consequently, deficient rainfall anomalies over the South China Sea and the northwestern Pacific are generated. The temperature advection anomalies are in accordance with the wind anomalies in both the summer mean and individual months (figures not shown).

As a result, both of the warm advection anomalies of temperature by anomalous westerly winds and the advection of anomalous positive relative vorticity by northerly basic winds cause anomalous ascending motion over the mei-yu–changma–baiu rainfall area, while the cold temperature advection anomalies by anomalous easterly winds and the advections of negative vorticity by the northerly basic winds lead to anomalous descending motion over the South China Sea area.

7. Discussion and summary

a. Discussion

From the perspective of thermal wind, the upper-level jet stream can reflect the thermal contrast between the north and south, and this is closely related to the strength of the EASM. This proves from another point of view that upper-level wind change is closely related to the EASM variability.

The formation and variability of the EASM is related to both tropical and the extratropical factors, and the NEWI is closely linked to both tropical (the SST) and extratropical factors (e.g., temperature over the Tibetan Plateau). This is due to the consideration of the wind anomalies not only in the northern and central areas, but also in the south. In the study of the East Asian winter monsoon (EAWM), some researchers divide the EAWM into northern and southern components since the northern and southern areas are mainly affected by different factors (Wang et al. 2010; Chen et al. 2014). Wu et al. (2008) have revealed that a single index of EASM is inappropriate for investigating and predicting the EASM, and it is difficult to distinguish which part (the tropical or the extratropical factors) matters more in the EASM variability using only one index. So in the following works we can also divide the EASM into two modes so as to perform more detailed and in-depth research and have further understanding of the EASM.

In the prediction of the EASM, from the perspective of atmospheric circulation, Zhang et al. (2003) studied the intensity change of EASM and found that the intensity of EASM is associated with the zonal wind's variability in the midlatitude ranges of Asia and the eastern Pacific area in the previous winter and spring. So they defined a precursor index using the 200-hPa zonal

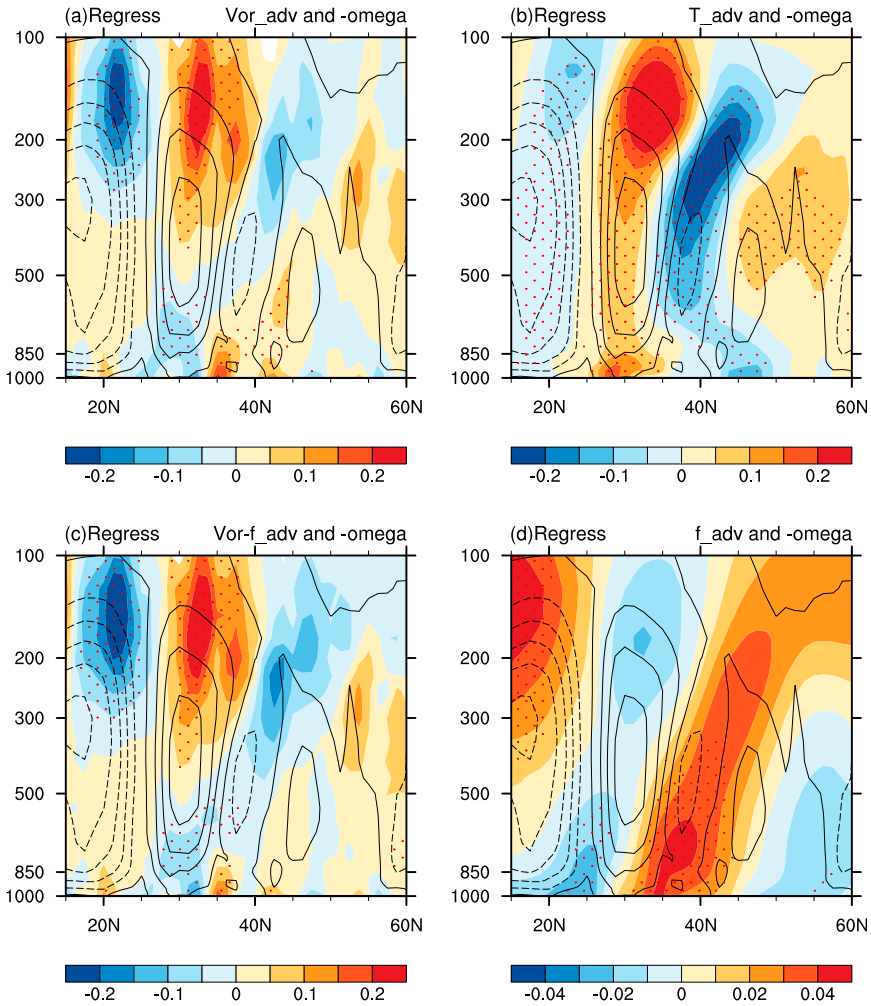

FIG. 12. (a) Latitude–height cross section showing the horizontal advection anomalies (color) of geostrophic absolute vorticity ($10^{-10}\,s^{-2}$; color shading) and upward vertical pressure velocity anomalies (black contours at every 0.2 hPa s^{-1}, negative values dashed) averaged between 105°–140°E regressed onto NEWI in JJA. (b)–(d) As in (a), but for temperature (K day^{-1}), relative vorticity ($10^{-10}\,s^{-2}$), and planetary vorticity ($10^{-10}\,s^{-2}$), respectively. The time period is 1958–2013. The red dots indicate the 95% confidence levels for the horizontal advection anomalies of geostrophic vorticity and temperature based on a two-sided Student's *t* test.

wind anomaly in the previous February. Following their work, we also find that when the zonal wind anomaly is negative around Asia and the tropical eastern Pacific in the previous winter, there is likely a strong EASM with sufficient mei-yu–changma–baiu rainfall. Many important atmospheric circulation predictors can be used to predict the EASM; for example, previous atmospheric circulation situations such as the North Atlantic Oscillation can impact the EASM, which is useful for the prediction of the EASM and deserves further investigation. Furthermore, for the prediction of the EASM, there is a mutation in the mid-1970s, but the reason is not clear and further investigation is needed. The processes by which how different ocean regions affect the EASM variability also need further study. In addition, in the model simulations of the EASM we have also examined simulation of the EASM at different lead times and found a relative good performance of the models when the lead time is shorter.

For the mechanism of EASM's decadal variability, there is still no consensus in the monsoon study. Zhu et al. (2012) found that global warming is likely responsible for the weakening of the northern EASM after the 1970s; there are also studies suggesting that the anthropogenic changes in atmospheric composition including greenhouse gases and aerosol emissions may also impact the EASM (Qian et al. 2009). Some researchers found that natural variability is the dominant

TABLE 3. Regression anomalies associated with the NEWI at 200 hPa (10^{-19} m s^{-1} kg^{-1}) for seven terms of B denoted by B1–B7 and six terms of C denoted by C1–C6 from Eq. (2) averaged over 30°–37.5°N, 105°–140°E and 15°–22.5°N, 105°–140°E.

Region	B1	B2	B3	B4	B5	B6	B7	C1	C2	C3	C4	C5	C6
30°–37.5°N, 105°–140°E	−0.28	0.11	0.02	0.14	2.47	0.09	0.24	1.65	0.47	0.01	0.13	0.19	0.04
15°–22.5°N, 105°–140°E	0.13	0.07	0.01	−0.07	−1.03	−0.06	0.13	−0.36	−0.08	−0.01	0.21	0.19	−0.01

factor in the decadal variability of EASM (Jiang and Wang 2005; Song et al. 2014). The decadal variability of the EASM involves both anthropogenic and natural variability.

Yun et al. (2010) investigated the interdecadal change in the relationship between ENSO and the intraseasonal oscillation in East Asia. Kim and Ha (2015) investigated the changes in the observed precipitation and moisture transport induced by anthropogenic forcing and natural variability. Song et al.'s (2014) research found that Pacific decadal oscillation plays an important role in regulating the EASM–ENSO relationship in the twentieth century. Wu et al. (2012) found that spring NAO may exert notable impacts on the enhancement of the EASM–ENSO relationship. Ding et al. (2010) have investigated the changes in the interannual relationship between the EASM and the TIO in the late 1970s. Previous studies have revealed two reasons for the decadal change of the relationship between TIO and EASM after the late 1970s: the southwestern Indian Ocean thermocline and ENSO (Xie et al. 2010; Hu et al. 2014). Huang et al. (2010) found that the strengthened TIO teleconnection to the northwestern Pacific since the mid-1970s coincides with an intensification of summer SST variability over the TIO. The decadal relationship between the EASM and SST (TIO and TEP) is influenced by many factors. How the anthropogenic and natural aspects matter needs further investigation.

As the mei-yu, changma, and baiu have distinct phases within intraseasonal time scale, some researches have investigated the intraseasonal features of the EASM. Chu et al. (2012) and Oh and Ha (2015) use various self-organizing maps node analysis to distinguish four major intraseasonal phases of the EASM (the mei-yu–baiu phase, the changma phase, the post-changma phase, and the dry-spell phase) and analyze these in more detail. They find that these modes have significant thermodynamic characteristics that are linked to the upper-level jet. Our study also indicates that the NEWI-related rain belts along with the NEWI-related vorticity advection anomalous centers and temperature advection anomalous centers in the upper level shift northward from June to August. This indicates that the NEWI may be used to study the intraseasonal variations of the EASM. Therefore, it is worthwhile to explore how the NEWI can capture the intraseasonal variation and climate features of the EASM in the future works. This may be another useful method for the seasonal prediction of the EASM variability.

In addition, from the precipitation and atmospheric circulation, the EASM shows an intimate relationship with atmospheric teleconnection pattern such as the EAP or PJ pattern. However, the detailed relationship between them has not been studied, which is another important topic in our future research.

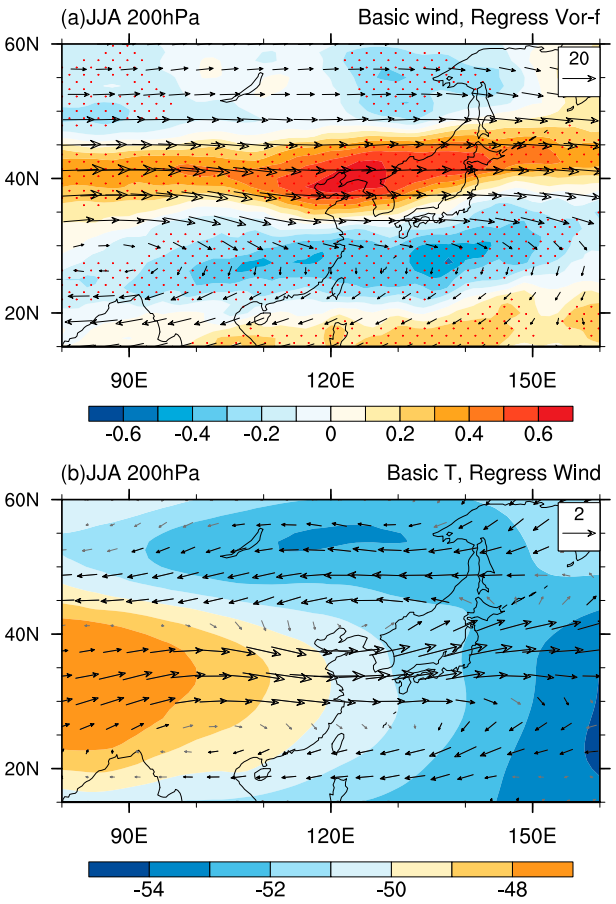

FIG. 13. (a) The 200-hPa mean horizontal wind (m s^{-1}; vectors) averaged in JJA with regression anomalies of 200-hPa relative vorticity (10^{-5} s^{-1}; color shading) against the JJA-mean NEWI. (b) The 200-hPa mean temperature (°C; color shading) averaged in JJA with regression anomalies of 200-hPa horizontal wind (m s^{-1}; vectors) against the NEWI. The time period is 1958–2013. The red dots in (a) and thick black vectors in (b) indicate the 95% confidence levels based on a two-sided Student's t test.

b. Summary

As indicated by previous works, the upper-level wind changes are closely connected to the climate anomalies over East Asia. In this paper, we analyze the 200-hPa zonal wind field and define a new EASM index by taking into account wind anomalies not only in the northern and central areas but also in the south. Following the suggestion by Wang et al. (2008), a strong EASM indicates an excessive rainfall in the mei-yu–changma–baiu area. The defined index captures the interannual and interdecadal variability well.

Compared with 15 indices defined by previous studies based on different variables, the NEWI has a good correlation with precipitation and temperature, and it can capture the dominant modes of rainfall and temperature. In addition, the NEWI captures the seasonal shift of the mei-yu–changma–baiu rain belt, and it can show the distinct climate anomalous features of early and late summer. From the circulation field, there exists an anomalous anticyclone in the northwestern Pacific during the strong EASM. The 500-hPa geopotential height anomalies show the EAP or PJ teleconnection pattern. Hence the NEWI reproduces the large-scale circulation of the EASM at the lower, middle, and upper troposphere well.

Then the predictability of the NEWI is explored and the ocean is an important origin for the predictability of the EASM. The two AGCMs, CAM3 and ECHAM5, both reproduce the NEWI well, indicating a vital role of ocean in the variability of the EASM. The tropical eastern Pacific SST shows a 4-month lead and the north Indian Ocean SST has a 1-month lead in predicting the EASM. Furthermore, the models predict well the EASM variations measured by the NEWI.

The physical mechanism of the EASM variability based on the NEWI is also analyzed. As rainfall anomalies are highly correlated with vertical motions, we use the quasigeostrophic omega equation to diagnose the formation mechanism of vertical motions. Precipitation can release condensational heating, which will reinforce upward movement, and then produce more precipitation in turn. In the variation of vorticity advection associated with the EASM, relative vorticity plays a vital role. When a strong EASM occurs, there are negative vorticity advection anomalies over about 15°–25°N in the upper level, leading to descending motions, and positive vorticity advection anomalies over 25°–35°N in the upper level lead to ascending motions.

The horizontal temperature advection anomalies associated with the upper-level wind over the Tibetan Plateau play an important role in the EASM area. The region of upward motion anomalies closely follows the region of warm temperature advection anomalies. When a strong EASM occurs, the NEWI is positive with westerly anomalies around 30°–40°N, leading to anomalous warm temperature advection, resulting in sufficient mei-yu–changma–baiu rainfall. On the other hand, there are easterly anomalies around 20°N, inducing cold advection anomalies to the south of China and over the South China Sea and the northwestern Pacific and deficient precipitation. Therefore, the vorticity advection anomalies and temperature advection anomalies in the upper level induce the vertical movement anomalies, causing the precipitation and temperature anomalies. In detail, both the warm advection anomalies of temperature by anomalous westerly winds and the advection of anomalous positive relative vorticity by northerly basic winds cause anomalous ascending motion over the mei-yu–changma–baiu rainfall area, while the cold temperature advection anomalies by anomalous easterly winds and the advections of the negative vorticity by northerly basic winds lead to anomalous descending motion over the South China Sea area.

Overall, the NEWI captures seasonal, interannual, and interdecadal variations of the EASM with a good representation of the related precipitation and temperature variations. It can also be predicted well both in observation and model simulation, and the physical mechanism is explicit. Therefore, the NEWI is a good choice to characterize the EASM and its associated climate.

Acknowledgments. This work was supported by the National Basic Research Program of China (2012CB955604), the National Science Foundation of China (91337105, 41425019, 41275083, and 41205049), Public Science and Technology Research Funds Projects of Ocean (201505013), and Project PAEKL-2014-K2.

REFERENCES

Chang, C.-P., Y. Zhang, and T. Li, 2000: Interannual and interdecadal variations of the East Asian summer monsoon and tropical Pacific SSTs. Part I: Roles of the subtropical ridge. *J. Climate*, **13**, 4310–4325, doi:10.1175/1520-0442(2000)013<4310:IAIVOT>2.0.CO;2.

Chen, L., M. Dong, and Y. N. Shao, 1992: The characteristics of interannual variations on the East Asian monsoon. *J. Meteor. Soc. Japan*, **70**, 397–421.

Chen, M., P. Xie, J. E. Janowiak, and P. A. Arkin, 2002: Global land precipitation: A 50-yr monthly analysis based on gauge observations. *J. Hydrometeor.*, **3**, 249–266, doi:10.1175/1525-7541(2002)003<0249:GLPAYM>2.0.CO;2.

Chen, T.-J. G., and C.-P. Chang, 1980: The structure and vorticity budget of an early summer monsoon trough (mei-yu) over

southeastern China and Japan. *Mon. Wea. Rev.*, **108**, 942–953, doi:10.1175/1520-0493(1980)108<0942:TSAVBO>2.0.CO;2.

Chen, Z., R. G. Wu, and W. Chen, 2014: Distinguishing interannual variations of the northern and southern modes of the East Asian winter monsoon. *J. Climate*, **27**, 835–851, doi:10.1175/JCLI-D-13-00314.1.

Chu, J.-E., S. N. Hameed, and K.-J. Ha, 2012: Nonlinear, intraseasonal phases of the East Asian summer monsoon: Extraction and analysis using self-organizing maps. *J. Climate*, **25**, 6975–6988, doi:10.1175/JCLI-D-11-00512.1.

Collins, W. D., and Coauthors, 2006: The Community Climate System Model version 3 (CCSM3). *J. Climate*, **19**, 2122–2143, doi:10.1175/JCLI3761.1.

Dai, A., H. Li, Y. Sun, L. Hong, LinHo, C. Chou, and T. J. Zhou, 2013: The relative roles of upper and lower tropospheric thermal contrasts and tropical influences in driving Asian summer monsoons. *J. Geophys. Res. Atmos.*, **118**, 7024–7045, doi:10.1002/jgrd.50565.

Dai, N., A. Xie, and Y. Zhang, 2000: Interannual and interdecadal variations of summer monsoon activities over South China Sea. *Climate Environ. Res.*, **5**, 363–374.

Ding, R., K.-J. Ha, and J. Li, 2010: Interdecadal shift in the relationship between the East Asian summer monsoon and the tropical Indian Ocean. *Climate Dyn.*, **34**, 1059–1071, doi:10.1007/s00382-009-0555-2.

Doblas-Reyes, F. J., and Coauthors, 2009: Addressing model uncertainty in seasonal and annual dynamical ensemble forecasts. *Quart. J. Roy. Meteor. Soc.*, **135**, 1538–1559, doi:10.1002/qj.464.

Du, Y., Y. Zhang, and Z. Xie, 2008: Impacts of longitude location changes of East Asian westerly jet core on the precipitation distribution during meiyu period in middle-lower reaches of Yangtze River valley. *Acta Meteor. Sin.*, **66**, 566–576.

Guo, Q., 1983: The summer monsoon intensity index in East Asia and its variation (in Chinese). *Acta Geogr. Sin.*, **38**, 207–217.

Ha, K.-J., S.-K. Park, and K.-Y. Kim, 2005: On interannual characteristics of Climate Prediction Center merged analysis precipitation over the Korean peninsula during the summer monsoon season. *Int. J. Climatol.*, **25**, 99–116, doi:10.1002/joc.1116.

He, J., J. Ju, Z. Wen, J. Lu, and Q. Jin, 2007: A review of recent advances in research on Asian monsoon in China. *Adv. Atmos. Sci.*, **24**, 972–992, doi:10.1007/s00376-007-0972-2.

Hirota, N., and M. Takahashi, 2012: A tripolar pattern as an internal mode of the East Asian summer monsoon. *Climate Dyn.*, **39**, 2219–2238, doi:10.1007/s00382-012-1416-y.

Hsu, H.-H., T. Zhou, and J. Matsumoto, 2014: East Asian, Indochina and western north Pacific summer monsoon—An update. *Asia-Pac. J. Atmos. Sci.*, **50**, 45–68, doi:10.1007/s13143-014-0027-4.

Hu, K., G. Huang, and R. Huang, 2011: The impact of tropical Indian Ocean variability on summer surface air temperature in China. *J. Climate*, **24**, 5365–5377, doi:10.1175/2011JCLI4152.1.

——, ——, and R. Wu, 2013: A strengthened influence of ENSO on August high temperature extremes over the southern Yangtze River valley since the late 1980s. *J. Climate*, **26**, 2205–2221, doi:10.1175/JCLI-D-12-00277.1.

——, ——, X.-T. Zheng, S. P. Xie, X. Qu, Y. Du, and L. Liu, 2014: Interdecadal variations in ENSO influences on northwest Pacific–East Asian early summertime climate simulated in CMIP5 models. *J. Climate*, **27**, 5982–5998, doi:10.1175/JCLI-D-13-00268.1.

Huang, G., and Z. Yan, 1999: The East Asian summer monsoon circulation anomaly index and its interannual variations. *Chin. Sci. Bull.*, **44**, 1325–1329, doi:10.1007/BF02885855.

——, K. Hu, and S.-P. Xie, 2010: Strengthening of tropical Indian Ocean teleconnection to the northwest Pacific since the mid-1970s: An atmospheric GCM study. *J. Climate*, **23**, 5294–5304, doi:10.1175/2010JCLI3577.1.

Huang, R., and Y. Wu, 1989: The influence of ENSO on the summer climate change in China and its mechanism. *Adv. Atmos. Sci.*, **6**, 21–32, doi:10.1007/BF02656915.

——, J. Chen, L. Wang, and Z. Lin, 2012: Characteristics, processes, and causes of the spatio-temporal variabilities of the East Asian monsoon system. *Adv. Atmos. Sci.*, **29**, 910–942, doi:10.1007/s00376-012-2015-x.

Jiang, D., and H. Wang, 2005: Natural interdecadal weakening of East Asian summer monsoon in the late 20th century. *Chin. Sci. Bull.*, **50**, 1923–1929, doi:10.1360/982005-36.

Jiang, T., Z. W. Kundzewicz, and B. Su, 2008: Changes in monthly precipitation and flood hazard in the Yangtze River basin, China. *Int. J. Climatol.*, **28**, 1471–1481, doi:10.1002/joc.1635.

Kim, B.-H., and K.-J. Ha, 2015: Observed changes of global and western Pacific precipitation associated with global warming SST mode and mega-ENSO SST mode. *Climate Dyn.*, doi:10.1007/s00382-015-2524-2, in press.

Kobayashi, S., and Coauthors, 2015: The JRA-55 Reanalysis: General specifications and basic characteristics. *J. Meteor. Soc. Japan*, **93**, 5–48, doi:10.2151/jmsj.2015-001.

Kosaka, Y., and H. Nakamura, 2010: Mechanisms of meridional teleconnection observed between a summer monsoon system and a subtropical anticyclone. Part I: The Pacific–Japan pattern. *J. Climate*, **23**, 5085–5108, doi:10.1175/2010JCLI3413.1.

Kwon, M., J.-G. Jhun, and K.-J. Ha, 2007: Decadal change in East Asian summer monsoon circulation in the mid-1990s. *Geophys. Res. Lett.*, **34**, L21706, doi:10.1029/2007GL031977.

Lau, K.-M., and M.-T. Li, 1984: The monsoon of East Asia and its global associations—A survey. *Bull. Amer. Meteor. Soc.*, **65**, 114–125, doi:10.1175/1520-0477(1984)065<0114:TMOEAA>2.0.CO;2.

——, K.-M. Kim, and S. Yang, 2000: Dynamical and boundary forcing characteristics of regional components of the Asian summer monsoon. *J. Climate*, **13**, 2461–2482, doi:10.1175/1520-0442(2000)013<2461:DABFCO>2.0.CO;2.

Lee, E.-J., J.-G. Jhun, and C.-K. Park, 2005: Remote connection of the northeast Asian summer rainfall variation revealed by a newly defined monsoon index. *J. Climate*, **18**, 4381–4393, doi:10.1175/JCLI3545.1.

Li, C., and M. Yanai, 1996: The onset and interannual variability of the Asian summer monsoon in relation to land–sea thermal contrast. *J. Climate*, **9**, 358–375, doi:10.1175/1520-0442(1996)009<0358:TOAIVO>2.0.CO;2.

——, J. Wang, S. Lin, and H. Cho, 2004: The relationship between East Asian summer monsoon activity and northward jump of the upper westerly jet location (in Chinese). *Chin. J. Atmos. Sci.*, **28**, 641–658.

Li, C. F., R. Lu, and B. Dong, 2012: Predictability of the western North Pacific summer climate demonstrated by the coupled models of ENSEMBLES. *Climate Dyn.*, **39**, 329–346, doi:10.1007/s00382-011-1274-z.

Li, Y., J. Li, and J. Feng, 2013: Boreal summer convection oscillation over the Indo-western Pacific and its relationship with

the East Asian summer monsoon. *Atmos. Sci. Lett.*, **14**, 66–71, doi:10.1002/asl2.418.

Liang, X.-Z., and W.-C. Wang, 1998: Associations between China monsoon rainfall and tropospheric jets. *Quart. J. Roy. Meteor. Soc.*, **124**, 2597–2623, doi:10.1002/qj.49712455204.

Lin, Z., and R. Lu, 2009: The ENSO's effect on eastern China rainfall in the following early summer. *Adv. Atmos. Sci.*, **26**, 333–342, doi:10.1007/s00376-009-0333-4.

Liu, H., T. Zhou, Y. Zhu, and Y. Lin, 2012: The strengthening East Asia summer monsoon since the early 1990s. *Chin. Sci. Bull.*, **57**, 1553–1558, doi:10.1007/s11434-012-4991-8.

Murakami, T., and J. Matsumoto, 1994: Summer monsoon over the Asian continent and western north Pacific. *J. Meteor. Soc. Japan*, **72**, 719–745.

Nitta, T., 1987: Convective activities in the tropical western Pacific and their impact on the Northern Hemisphere summer circulation. *J. Meteor. Soc. Japan*, **65**, 373–390.

Oh, H., and K.-J. Ha, 2015: Thermodynamic characteristics and responses to ENSO of dominant intraseasonal modes in the East Asian summer monsoon. *Climate Dyn.*, **44**, 1751–1766, doi:10.1007/s00382-014-2268-4.

Peixóto, J. P., and A. H. Oort, 1984: Physics of climate. *Rev. Mod. Phys.*, **56**, 365, http://dx.doi.org/10.1103/RevModPhys.56.365.

Peng, J., Z. Sun, and D. Ni, 2000: Relation of eastern Asian summer monsoon with the equatorial eastern Pacific spring SSTA (in Chinese). *J. Nanjing Inst. Meteor.*, **23**, 385–390.

Qian, Y., D. Gong, J. Fan, L. R. Leung, R. Bennartz, D. Chen, and W. Wang, 2009: Heavy pollution suppresses light rain in China: Observations and modeling. *J. Geophys. Res.*, **114**, D00K02, doi:10.1029/2008JD011575.

Qu, X., and G. Huang, 2012: Impacts of tropical Indian Ocean SST on the meridional displacement of East Asian jet in boreal summer. *Int. J. Climatol.*, **32**, 2073–2080, doi:10.1002/joc.2378.

Rodwell, M. J., and B. J. Hoskins, 2001: Subtropical anticyclones and summer monsoons. *J. Climate*, **14**, 3192–3211, doi:10.1175/1520-0442(2001)014<3192:SAASM>2.0.CO;2.

Sampe, T., and S.-P. Xie, 2010: Large-scale dynamics of the meiyu-baiu rainband: Environmental forcing by the westerly jet. *J. Climate*, **23**, 113–134, doi:10.1175/2009JCLI3128.1.

Shen, S., and K.-M. Lau, 1995: Biennial oscillation associated with the East-Asian summer monsoon and tropical sea-surface temperatures. *J. Meteor. Soc. Japan*, **73**, 105–124.

Shi, N., and Q. G. Zhu, 1996: An abrupt change in the intensity of the East Asian summer monsoon index and its relationship with temperature and precipitation over east China. *Int. J. Climatol.*, **16**, 757–764, doi:10.1002/(SICI)1097-0088(199607)16:7<757::AID-JOC50>3.0.CO;2-5.

Smith, T. M., R. W. Reynolds, T. C. Peterson, and J. Lawrimore, 2007: Improvements to NOAA's historical merged land–ocean surface temperature analysis (1880–2006). *J. Climate*, **21**, 2283–2296, doi:10.1175/2007JCLI2100.1.

Song, F., T. Zhou, and Y. Qian, 2014: Responses of East Asian summer monsoon to natural and anthropogenic forcings in the 17 latest CMIP5 models. *Geophys. Res. Lett.*, **41**, 596–603, doi:10.1002/2013GL058705.

Tao, S., and L. Chen, 1957: The structure of general circulation over continent of Asia in summer. *Acta Meteor. Sin.*, **28**, 234–247.

——, and J. Wei, 2006: The westward and northward advance of the subtropical high over the west Pacific in summer (in Chinese). *J. Appl. Meteor. Sci.*, **17**, 513–525.

Wang, B., and Z. Fan, 1999: Choice of South Asian summer monsoon indices. *Bull. Amer. Meteor. Soc.*, **80**, 629–638, doi:10.1175/1520-0477(1999)080<0629:COSASM>2.0.CO;2.

——, R. Wu, and X. Fu, 2000: Pacific–East Asian teleconnection: How does ENSO affect East Asian climate? *J. Climate*, **13**, 1517–1536, doi:10.1175/1520-0442(2000)013<1517:PEATHD>2.0.CO;2.

——, ——, and K.-M. Lau, 2001: Interannual variability of the Asian summer monsoon: Contrasts between the Indian and the western north Pacific–East Asian monsoons. *J. Climate*, **14**, 4073–4090, doi:10.1175/1520-0442(2001)014<4073:IVOTAS>2.0.CO;2.

——, Z. Wu, J. Li, J. Liu, C.-P. Chang, Y. Ding, and G. Wu, 2008: How to measure the strength of the East Asian summer monsoon. *J. Climate*, **21**, 4449–4463, doi:10.1175/2008JCLI2183.1.

——, J. Liu, J. Yang, T. Zhou, and Z. W. Wu, 2009: Distinct principal modes of early and late summer rainfall anomalies in East Asia. *J. Climate*, **22**, 3864–3875, doi:10.1175/2009JCLI2850.1.

——, Z. Wu, C.-P. Chang, J. Liu, J. Li, and T. Zhou, 2010: Another look at interannual-to-interdecadal variations of the East Asian winter monsoon: The northern and southern temperature modes. *J. Climate*, **23**, 1495–1512, doi:10.1175/2009JCLI3243.1.

Wang, Y., B. Wang, and J.-H. Oh, 2001: Impact of the preceding El Nino on the East Asian summer atmosphere circulation. *J. Meteor. Soc. Japan*, **79**, 575–588, doi:10.2151/jmsj.79.575.

Webster, P. J., and S. Yang, 1992: Monsoon and ENSO: Selectively interactive systems. *Quart. J. Roy. Meteor. Soc.*, **118**, 877–926, doi:10.1002/qj.49711850705.

Wu, A., and Y. Ni, 1997: The influence of Tibetan Plateau on the interannual variability of Asian monsoon. *Adv. Atmos. Sci.*, **14**, 491–504, doi:10.1007/s00376-997-0067-0.

Wu, B., R. Zhang, Y. Ding, and R. D'Arrigo, 2008: Distinct modes of the East Asian summer monsoon. *J. Climate*, **21**, 1122–1138, doi:10.1175/2007JCLI1592.1.

Wu, R., J. Chen, and Z. Wen, 2013: Precipitation–surface temperature relationship in the IPCC CMIP5 models. *Adv. Atmos. Sci.*, **30**, 766–778, doi:10.1007/s00376-012-2130-8.

Wu, Z., J. Li, Z. Jiang, J. He, and X. Zhu, 2012: Possible effects of the North Atlantic Oscillation on the strengthening relationship between the East Asian summer monsoon and ENSO. *Int. J. Climatol.*, **32**, 794–800, doi:10.1002/joc.2309.

Xie, S.-P., K. Hu, J. Hafner, H. Tokinaga, Y. Du, G. Huang, and T. Sampe, 2009: Indian Ocean capacitor effect on Indo–western Pacific climate during the summer following El Niño. *J. Climate*, **22**, 730–747, doi:10.1175/2008JCLI2544.1.

——, Y. Du, G. Huang, X.-T. Zheng, H. Tokinaga, K. Hu, and Q. Liu, 2010: Decadal shift in El Niño influences on Indo-western Pacific and East Asian climate in the 1970s. *J. Climate*, **23**, 3352–3368, doi:10.1175/2010JCLI3429.1.

Yang, S., and P. J. Webster, 1990: The effect of summer tropical heating on the location and intensity of the extratropical westerly jet streams. *J. Geophys. Res.*, **95**, 18 705–18 721, doi:10.1029/JD095iD11p18705.

Yun, K.-S., K.-H. Seo, and K.-J. Ha, 2008: Relationship between ENSO and northward propagating intraseasonal oscillation in the East Asian summer monsoon system. *J. Geophys. Res.*, **113**, D14120, doi:10.1029/2008JD009901.

——, ——, and ——, 2010: Interdecadal change in the relationship between ENSO and the intraseasonal oscillation in East Asia. *J. Climate*, **23**, 3599–3612, doi:10.1175/2010JCLI3431.1.

Zhang, Q., S. Tao, and L. Chen, 2003: The inter-annual variability of East Asian summer monsoon indices and its association with the pattern of general circulation over East Asia (in Chinese). *Acta Meteor. Sin.*, **61**, 559–568.

Zhang, Y., and X. Kuang, 2006: Simulation of seasonal variation of the East Asian subtropical westerly jet in a coupled climate system model FGCM0. *Chin. J. Atmos. Sci.*, **30**, 1177–1188.

——, ——, W. Guo, and T. Zhou, 2006: Seasonal evolution of the upper-tropospheric westerly jet core over East Asia. *Geophys. Res. Lett.*, **33**, L11708, doi:10.1029/2006GL026377.

Zhao, P., and Z. Zhou, 2009: An East Asian subtropical summer monsoon index and its relationship to summer rainfall in China. *Acta Meteor. Sin.*, **23**, 18–28.

Zhou, T., D. Gong, J. Li, and B. Li, 2009: Detecting and understanding the multi-decadal variability of the East Asian summer monsoon—Recent progress and state of affairs. *Meteor. Z.*, **18**, 455–467, doi:10.1127/0941-2948/2009/0396.

Zhu, C., H. Jinhai, and W. Guoxiong, 2000: East Asian monsoon index and its interannual relationship with large-scale thermal dynamic circulation. *Acta Meteor. Sin.*, **58**, 391–402.

Zhu, C. W., B. Wang, W. H. Qian, and B. Zhang, 2012: Recent weakening of northern East Asian summer monsoon: A possible response to global warming. *Geophys. Res. Lett.*, **39**, L09701, doi:10.1029/2012GL051155.